

Response to Anonymous Referee #3

The referee's comments are bolded and italicized while our comments are in plain text

The present work extends the knowledge on depositional and immersion mode freezing of ice on volcanic ash samples. Three selected ash samples have been chosen to study IN formation by Raman micro-spectroscopy. These samples cover the range of basaltic, andesitic and rhyolitic ash. While all three samples exhibit a similar behavior during depositional freezing, the authors claim varying behaviour during immersion mode freezing, which might be related to differences in the mineralogy of crystalline material. In contrast to previous studies, their results indicate, that a 'simple' parameterization of the immersion mode freezing for volcanic ashes is not legal. After a brief and straightforward introduction, a detailed experimental section is following. The results of their study are presented according to IN properties in the depositional and immersion mode. The paper concludes with a discussion on atmospheric implications. The paper is well written and could be interesting to the readership of Atmospheric Chemistry and Physics. However, the paper lacks of experimental details and interpretation of data obtained from Raman spectroscopy. Further, the significance of the results has to be discussed related to the limited dataset. Therefore, publication in ACP can only be considered after addressing the following major remarks in detail.

The author's would first like to thank anonymous referee #3 for his/her insightful comments that have improved the clarity of this manuscript

Major issues:

**) The title of the paper includes ". . . using Raman spectroscopy" – however, only Raman spectra related to depositional freezing are shown in figure 1. The authors claim, that their study is the first immersion mode freezing study, therefore it is absolutely important to discuss and display details of Raman spectra obtained during the immersion mode experiments in detail. Even experimental details have to be discussed like influence of laser power on heating of the droplets and disturbing the measurements and results. Further, for confocal Raman microscopy, height of the z-resolution must be discussed related to the sample size and height. How reliable are results from a single spot measurement of 20 to 70 μm droplets (see fig. 3)? A discussion about the legitimacy of Raman micro-spectroscopy for immersion mode measurements is absolutely necessary. For a reader, the experimental work appears in that way, that only the optical part of the microscope was used for obtaining the dataset, but not the Raman spectrometer.*

The authors thank the referee for making the valid point that we do not show any Raman spectra for the immersion freezing experiments. Unfortunately, this is because Raman spectroscopy was not utilized during immersion freezing experiments. This was largely because Raman spectra of water droplets containing volcanic ash or minerals were dominated by the -OH stretch due to liquid water. The authors agree that including the phrase "using Raman Spectroscopy" in the title may be misleading. Thus, the authors have removed the phrase "using Raman Spectroscopy" from the title.

****) The authors claim that up to now only two datasets have been used to suggest one characteristic ice nucleation efficiency. They extended the dataset from two to five ash samples. There is no statistical confidence within this interpretation. How can the authors reliably conclude that immersion mode freezing is dependent on the composition of the ash by this limited dataset?***

The authors agree that the immersion freezing of volcanic ash may not be entirely dependent on the composition of the ash. Thus, the following sentence has been added Page 1401, line 8:

“It is important to note that the above discussion interprets immersion freezing only from a chemical mechanism standpoint.”

****) How was sampling of the volcanic ashes done? Were the samples collected from the nearby ash fall around the volcanos? How long were the ashes exposed to environmental conditions after the eruptions of the related volcanos? Are particles which settle close to the volcano comparable with fly-ash which is able to cover a distance of several hundreds of kilometres? Is there a general independence of the chemical composition, environmental aging from the size and the difference in exposure (atmosphere, soil, . . .)?***

The authors agree that the volcanic ash sampling details were not sufficiently detailed. Thus, the paragraph start on page 1389, line 11 now reads:

“Volcanic ash was collected from three separate volcanic eruptions that produced three distinct types of ash. Volcan Fuego (14.4828° N, 90.8828° W) is an active stratovolcano that lies 16 km north of Antigua, Guatemala. The sub-Plinian eruption of October 14, 1974 produced ash fall that impacted an area of ~400 km², and samples used here were collected by previous researchers immediately after eruption from a location 10 km from the vent. The Soufrière Hills volcano (16.7167° N, 62.1833° W) is an active stratovolcano located in Montserrat, an island in the Lesser Antilles island arc of the West Indies. The ongoing eruption, which began in 1995, produces cyclic dome-building and explosive activity, with samples used here resulting from an explosion in January of 2010; samples were collected immediately after deposition < 3 km from the vent. Finally, the Taupo caldera (38.8056° S, 175.9008° E) sits in the center of the North Island of New Zealand. Samples used here were collected from air fall deposits of the Oruanui ultra-Plinian eruption ~26 ka. The samples were excavated 39 km from the vent 25.4 ka after the eruption.”

The authors also acknowledge that there may not be a general independence of chemical composition and due to distances from the vent or environmental aging; unfortunately, such questions probe complex chemical mechanisms that are beyond the scope of this work. To highlight this we have added the following sentence to Page 1390, line 7:

“Chemical differences due to collection distances from the vent or environmental aging were not explicitly taken into account in this study.”

General minor issues:

****) Raman spectra in figure 1 (and others): These Raman spectra are displayed like they were measured in the anti-Stokes mode. Are these anti-Stokes spectra or are the spectra displayed in***

an unusual way for Stokes-Raman spectra. Further, assignment of the Raman excitations would improve the quality of the figure and assist a detailed understanding of the work.

While the authors agree that the Raman spectra are displayed as if they were measured in the anti-Stokes mode, we have traditionally presented the Raman spectra from our Raman microscope in this orientation. This decision was made to accommodate readers in the fields of atmospheric chemistry and physics who, the authors assume, are generally more familiar with infrared spectroscopy. To clarify this, we have altered Page 1391, line 5 to now read “Stokes-mode Raman spectra.”

****) Sampling: Indication of the geo-coordinates of the volcanos and the sampling site as well as the distance from the sampling site to the craters would be helpful.***

See comments above about sampling.

Response to Zamin A. Kanji

The referee's comments are bolded and italicized while our comments are in plain text

This manuscript discusses the deposition and immersion mode ice nucleation behavior of three volcanic ash samples as well as Kaolinite (KGa-1b) and Na/Ca Feldspar as references. The data presented is of timely interest to the readers of ACP, in particular the ice nucleation community. The methods used are sound and have been validated before in previous publications. The major conclusion is that not all volcanic ash samples have the same ice nucleation activity in immersion mode. In addition, Na/Ca Feldspar content was not found to be a good predictor of ice nucleation efficiency, rather it is proposed that the Silica (quartz) content would better explain the ice nucleation ranking behaviour of the ash samples in immersion freezing. The paper is written well and limitations are also discussed. I have suggested a few minor revisions, additions and have a few questions, all indicated directly in the manuscript. I recommend the paper to be published after the minor comments are addressed.

The author's would first like to thank Dr. Kanji for his insightful comments that have improved the clarity of this manuscript

Specific Comments:

Page 1387, line 21: You could consider using INP, this is not necessary but something to consider in case you have not

While this is a valid suggestion that is prevalent in the ice nucleation literature, the authors prefer to use ice nuclei (IN) to ice-nucleating particles (INP) in order to differentiate between heterogeneous ice nuclei and particles that freeze homogeneously, as well as avoid confusion with the also-common "ice nucleation protein."

Page 1388, line 18: What type of classification, mineralogy or emission mass, content?

The authors agree that the phrase "similar classifications" is vague and perhaps inappropriate to use when comparing only two samples. Thus the text has been changed on Page 1388, line 18 to read "these results represent only two volcanoes."

Page 1388, line 23: Maybe some more information on what this means, for the readership of the paper. It may be obvious to geologists/volcanologists but maybe not to cloud microphysicists and atmospheric scientist.

The authors agree that this terminology may be unfamiliar to cloud microphysicists and atmospheric scientist who are the target audience for this paper. Thus, Page 1388, line 23 has now been changed to read "which are basaltic (45-52% SiO₂), andesitic (56-59% SiO₂), and rhyolitic ashes (63-75% SiO₂) (Heiken, 1972), respectively."

Page 1389, line 1: Would be nice to specify the type of Ka here. We know different batches have different IN activity in particular the samples from CMS are different from Fluka.

Given this papers focus on linking mineralogy to ice nucleation efficiency, the authors agree that the type of kaolinite should be specified here. Thus, Page 1389, line 1 now reads “kaolinite (KGa-1b, Sihvonen et al, 2014).”

Page 1389, lines 15-21: When was the sample conducted relative to the eruption? Date of samping?

The authors agree that both the location and sampling date provide important insights into the results of the study. Thus, the paragraph start on page 1389, line 11 now reads:

“Volcanic ash was collected from three separate volcanic eruptions that produced three distinct types of ash. Volcan Fuego (14.4828° N, 90.8828° W) is an active stratovolcano that lies 16 km north of Antigua, Guatemala. The sub-Plinian eruption of October 14, 1974 produced ash fall that impacted an area of ~400 km², and samples used here were collected by previous researchers immediately after eruption from a location 10 km from the vent. The Soufrière Hills volcano (16.7167° N, 62.1833° W) is an active stratovolcano located in Montserrat, an island in the Lesser Antilles island arc of the West Indies. The ongoing eruption, which began in 1995, produces cyclic dome-building and explosive activity, with samples used here resulting from an explosion in January of 2010; samples were collected immediately after deposition < 3 km from the vent. Finally, the Taupo caldera (38.8056° S, 175.9008° E) sits in the center of the North Island of New Zealand. Samples used here were collected from air fall deposits of the Oruanui ultra-Plinian eruption ~26 ka. The samples were excavated 39 km from the vent 25.4 ka after the eruption.”

Page 1392, line 10: Were there conditions at which ice formed on the fused-silica disc? If so, what were the temp and RH conditions when you observed this? And could this have occurred else where on the stage not under the field of view of the microscope

The authors agree that ice formation on the substrate could provide a significant artifact in the experiment and reporting the conditions at which this occurs is important. These results have been previously reported in Baustian et al., 2010. Thus the following line was added to Page 1392, line 10:

“We have previously reported the conditions under which a blank fused-silica disc initiates ice formation (Baustian et al., 2010). In that study, we found that the blank substrate nucleated ice at S_{ice} of 1.6 to 2.33 from ~235 to 215 K.”

Page 1393, line 26: Can you distinguish if the ice formed before the contact or the contact occurred before the ice nucleation? See comment at Figure 3.

The authors agree that care should be taken our immersion freezing analysis not to include contact freezing events. Such precautions were taken, and the text starting on Page 1393, line 26 has now been revised to read:

“Further, by recording 30 frame-per-second video, we could unambiguously determine if droplets coagulated or froze by contact freezing. In all experiments, no contact-freezing events occurred from the contact of two liquid drops. If two droplets coagulated, their coagulated droplet size was

considered. Unfrozen droplets, however, could be frozen by contact with growing ice particles; those contact-frozen droplets were disregarded in our analysis.”

Page 1394, line 21: What are the silica contents different in Table 1 and 2?

The authors acknowledge that the difference between silica content and quartz content was not sufficiently explained in the discussion paper. The silica content of the ash is determined from elemental analyses, most commonly as X-ray fluorescence, and will include Si contributions from the melt glass, minerals, and lithic materials in the ash. Quartz is a pure, crystalline form of SiO₂, and its content is determined from X-ray diffraction. To clarify this in the text, we have added the following sentences to Page 1390, line 1:

“It is important to note that silica content of the ash is determined from elemental analyses, most commonly as X-ray fluorescence, and will include Si contributions from the melt glass, minerals, and lithic materials in the ash; this is not to be confused with quartz, which can be one mineral component of the ash composed is pure, crystalline SiO₂.”

Page 1398, line 5: Why not calculate nucleation rates if you really would like to take time dependence into account? And compare nucleation rates to one another?

While the authors agree that calculating nucleation rates and comparing those nucleation rates to previous studies would indeed be taking time dependence into account, the focus of this exercise was to validate our immersion freezing setups with a material and framework (i.e., the singular approximation) used by both continuous flow and cold stage instruments. Finally, while an in-depth discussion of the time-dependence of heterogeneous ice nucleation would be an interesting area to explore, to fully analyze it is beyond the capabilities of this data set.

Page 1411: Why is the silica content here different from that in Table 1?

See comments above about silica content.

Page 1412: There is an appearance of a small peak in the ground and nebulized sample. What is this attributed to and shouldn't it be addressed.

The authors agree that there is a small peak near 663 cm⁻¹ that is present in the ground and the ground/nebulized samples, but not present in the unground samples. Since volcanic ash is a complex mixture of volcanic glass, minerals, and possibly lithic material, peak identification is outside of the scope of this manuscript. We do, however, postulate that this peak emerges due to better homogeneity of the ground samples. To highlight this, another vertical dashed line has been added to Figure 1 and the following passages have been altered in the manuscript to read:

Page 1391, line 20: “An example set of these spectra for Soufrière Hills ash is shown in Fig. 1. It can be seen that the main ash signatures at 507 cm⁻¹, 408 cm⁻¹, and 281 cm⁻¹ in the Raman spectra are not significantly altered between the unground, ground, and aggregated particles, indicating that any major chemical alteration due to ash processing was not detected for these samples. A small peak at 663 cm⁻¹, however, does appear in the ground and ground/nebulized and dried ash; we attribute this peak this better homogeneity of minor components within the ground samples as compared to the unground samples.”

Page 1412: “A set of example Raman spectra of unground, ground, and ground/nebulized Soufrière Hills volcanic ash. As shown, the main peaks at 507 cm^{-1} , 408 cm^{-1} , and 281 cm^{-1} (vertical dashed lines) are minimally affected by mechanical grinding and wet generation, suggesting that bulk chemical alteration does not occur. A small peak at 663 cm^{-1} , however, does appear in the ground samples, possibly due to better homogeneity of minor components when compared to unground samples.”

Page 1414: Is it possible to provide a more magnified version of this figure, where the lack of structure and appearance of a structure in the frozen droplets is more evident. It is not super clear in these figures. Although if one observed closely, the bottom figure does have a few crystals with protrusions that would imply ice formation.

Unfortunately, video recordings of the experiments were taken at 20x magnification in order to view a statistically significant number of particles within the image frame. Magnifying the images would not increase the level of detail within the image.

Page 1414: If the droplets continue to coagulate even after you have stopped depositing the particles on the stage and during the cooling process, this needs to be made clear. It is also evident from the images that in the liquid phase there are more droplets than in the image where ice is present. So is this only due to the bergeron-findeisen process or could it be from contact nucleation with the small droplets diffusing to the large ones as pointed out in the image.

See comments above about droplet coagulation and contact freezing.

Page 1415: Kelvin here, but degrees C in the next plot, then you switch back to Kelvin. Why? Can you just chose one and stick to it?

The authors agree that switching between the two temperature scales is confusing; however to better compare figures to previous work in the literature, we have kept all frozen fraction curves in the Celsius scale and all n_s and S_{ice} plots in the Kelvin scale.

Page 1419: Are these data points that cover homogeneous nucleation, if so, you may consider removing them from this plot. To me it looks like these drops based on plots from Figure 7, froze homogeneously, then I think that there is no need to plot them on an n_s curve, since the surface area should not matter for their freezing. This is also implicit by the steep slope. You may want to comment about the lack of temperature dependence or the different temperature dependence here for these data point.

The authors agree that the points below $\sim 238\text{ K}$ may be due to homogeneous freezing as indicated by their steep slope in Figure 8 and their coincidence with the homogeneous freezing curve in Figure 7. Thus, the temperature range on Figure 8 has been altered to truncate at 238 K .

Minor Changes

The word “for” has been added to Page 1387, line 4.

“Further” has been changed to “furthermore” on Page 1387, line 11.

The word “ice” has been deleted Page 1387, line 13.

The reference Hoyle et al., 2011 ACP has been added to Page 1388, line 4.

The phrase “in modifying the composition of the aerosolized ash” has been added to Page 1389, line 24.

The phrase “droplet size” has been added to Page 1393, line 22, so that it now reads “and 65-165 μm (droplets size, lateral diameter).”

The last sentence on Page 1393 has been changed for clarity. It now reads “The temperature error of 0.5 K for all droplets was determined by repeated homogeneous freezing experiments of ultra-pure water.”

The phrase “in the temperature range investigated” has been added to Page 1395, line 9.

The “Hiranuma et al., 2014a” reference on Page 1398, line 14 has been changed to “Hiranuma et al., 2015.” This has also been changed in the reference section.

Relevant Changes (Response to Referees)

Page 1, line 2: Deleted “using Raman Spectroscopy” from the title

Page 3, line 38: Added “for”

Page 3, line 46: “Further” now reads “furthermore”

Page 3, line 47: Deleted “ice”

Page 4, line 64: Added the reference “Hoyle et al., 2011”

Page 5, line 76: This sentence has been altered for clarity. It now reads “these results represent only two volcanoes.”

Page 5, line 81: This sentence has been altered for clarity. It now reads “which are basaltic (45-52% SiO₂), andesitic (56-59% SiO₂), and rhyolitic ashes (63-75% SiO₂) (Heiken, 1972), respectively.

Page 5, line 88: The type of clay, “KGa-1b,” has been specified.

Page 5, line 97: The paragraph starting here has been altered to provide a more detailed description of the ash sampling. It now reads

“Volcanic ash was collected from three separate volcanic eruptions that produced three distinct types of ash. Volcan Fuego (14.4828° N, 90.8828° W) is an active stratovolcano that lies 16 km north of Antigua, Guatemala. The sub-Plinian eruption of October 14, 1974 produced ash fall that impacted an area of ~400 km², and samples used here were collected by previous researchers immediately after eruption from a location 10 km from the vent. The Soufrière Hills volcano (16.7167° N, 62.1833° W) is an active stratovolcano located in Montserrat, an island in the Lesser Antilles island arc of the West Indies. The ongoing eruption, which began in 1995, produces cyclic dome-building and explosive activity, with samples used here resulting from an explosion in January of 2010; samples were collected immediately after deposition < 3 km from the vent. Finally, the Taupo caldera (38.8056° S, 175.9008° E) sits in the center of the North Island of New Zealand. Samples used here were collected from air fall deposits of the Oruanui ultra-Plinian eruption ~26 ka. The samples were excavated 39 km from the vent 25.4 ka after the eruption.”

Page 6, line 111: Added the phrase “in modifying the composition of the aerosolized ash.”

Page 6 line 114: Added the sentence “It is important to note that silica content of the ash is determined from elemental analyses, most commonly as X-ray fluorescence, and will include Si contributions from the melt glass, minerals, and lithic materials in the ash; this is not to be confused with quartz, which can be one mineral component of the ash composed is pure, crystalline SiO₂.”

Page 7, line 123: Added the sentence “Chemical differences due to collection distances from the vent or environmental aging were not explicitly taken into account in this study.”

Page 8, line 148: Added “Stokes-mode” to clarify the type of Raman spectra display

Page 8, line 164: The following sentences have been altered to account for a small peak at 663 cm^{-1} appearing in the ground spectra. It now reads

“It can be seen that the main ash signatures at 507 cm^{-1} , 408 cm^{-1} , and 281 cm^{-1} in the Raman spectra are not significantly altered between the unground, ground, and aggregated particles, indicating that any major chemical alteration due to ash processing was not detected for these samples. A small peak at 663 cm^{-1} , however, does appear in the ground and ground/nebulized and dried ash; we attribute this peak to the better homogeneity of minor components within the ground samples as compared to the unground samples.”

Page 9, line 180: Added the following sentence: “We have previously reported the conditions under which a blank fused-silica initiates ice formation (Baustian et al., 2010). In that study, we found that the blank substrate nucleated ice at S_{ice} of 1.6 to 2.33 from ~ 235 to 215 K .”

Page 11, line 217: Added “droplet size”

Page 11, line 220: The following sentences were altered to clarify that, in our experiments, we can distinguish between immersion and contact freezing. These sentences now read

“Further, by recording 30 frame-per-second video, we could unambiguously determine if droplets coagulated or froze by contact freezing. In all experiments, no contact-freezing events occurred from the contact of two liquid drops. If two droplets coagulated, only their coagulated droplet size was considered. Unfrozen droplets, however, could be frozen by contact with growing ice particles; those contact-frozen droplets were disregarded in our analysis. Errors in n_s values are based on the range of surface areas available in each experiment. The temperature error of 0.5 K for all droplets was determined by repeated homogeneous freezing experiments of ultra-pure water.”

Page 12, line 256: The phrase “in the temperature range investigated” was added.

Page 16, line 333: Hiranuma et al., 2014b has been changed to Hiranuma et al., 2015

Page 17, line 362: Hiranuma et al., 2014b has been changed to Hiranuma et al., 2015

Page 19, line 403: Added the sentence “It is important to note that the above discussion interprets immersion freezing only from a chemical mechanism standpoint.”

Page 26, line 501: Figure 1 was altered to contain an additional vertical dashed line at 663 cm^{-1}

Page 26, line 505: Added the following sentence to the caption of Figure 1: “A small peak at 663 cm^{-1} , however, does appear in the ground samples, possibly due to better homogeneity of minor components when compared to unground samples.”

Page 34, line 540: Figure 8 was altered such that the right hand side of the x-axis ends at 238.15 K

Page 37, line 596: Altered the Hiranuma et al., 2014b ACPD reference to be the Hiranuma et al., 2015 ACP reference.

Relevant Changes (Authors Decision):

Page 10, line 203: The blank substrate was erroneously labeled “quartz.” It has now been changed to “fused silica.”

Page 18, line 394: In light of recent work published by Zolles et al., (2015), the following line was deleted: “To our knowledge, a laboratory standard of Na/Ca-feldspar cannot be obtained without these K-feldspar impurities.”

Page 18, line 397: In light of recent work published by Zolles et al., (2015), the following line was added: “This is in agreement with Zolles et al. (2015), who found that the Na/Ca-feldspars albite and anorthian andesine as well as an albite-dominated ash sample were all weak immersion-mode IN.”

Page 22, line 477: In the discussion manuscript, the authors had missed an important reference by Seifert et al., 2011. In light of this, we have added

“Furthermore, a study using polarization lidars at two central-European stations found a clear influence of volcanic ash on heterogeneous ice nucleation of tropospheric clouds. For example, in that study, all observed cloud layers with cloud top temperatures < -15 C contained ice during the days following the April 2010 Eyjafjallajökull volcanic eruption (Seifert et al., 2011).”

Page 40, line 684: Added the Seifert et al., 2011 reference to the reference section.

Page 41, line 725: Added the Zolles et al., 2015 reference to the reference section.

1 Deposition and Immersion Mode Nucleation of Ice by Three 2 Distinct Samples of Volcanic Ash ~~Using Raman Spectroscopy~~

3
4 **Gregory P. Schill^{1,*}, Kimberly Genareau², and Margaret A. Tolbert¹**

5 [1]{Department of Chemistry and Biochemistry and Cooperative Institute for Research in
6 Environmental Science, University of Colorado, Boulder, CO, USA }

7 [2]{Department of Geological Sciences, University of Alabama, Tuscaloosa, AL, USA }

8 [*]{Now at Department of Atmospheric Sciences, Colorado State University, Fort Collins, CO,
9 USA }

10 Correspondence to: M.A. Tolbert (tolbert@colorado.edu)

11 12 **Abstract**

13 Ice nucleation on volcanic ash controls both ash aggregation and cloud glaciation, which affect
14 atmospheric transport and global climate. Previously, it has been suggested that there is one
15 characteristic ice nucleation efficiency for all volcanic ash, regardless of its composition, when
16 accounting for surface area; however, this claim is derived from data from only two volcanic
17 eruptions. In this work, we have studied the depositional and immersion freezing efficiency of
18 three distinct samples of volcanic ash using Raman Microscopy coupled to an environmental cell.
19 Ash from the Fuego (basaltic ash, Guatemala), Soufrière Hills (andesitic ash, Montserrat), and
20 Taupo (Oruanui eruption, rhyolitic ash, New Zealand) volcanoes were chosen to represent different
21 geographical locations and silica content. All ash samples were quantitatively analyzed for both
22 percent crystallinity and mineralogy using X-ray diffraction. In the present study, we find that all
23 three samples of volcanic ash are excellent depositional ice nuclei, nucleating ice from 225-235 K

24 at ice saturation ratios of 1.05 ± 0.01 , comparable to the mineral dust proxy kaolinite. Since
25 depositional ice nucleation will be more important at colder temperatures, fine volcanic ash may
26 represent a global source of cold-cloud ice nuclei. For immersion freezing relevant to mixed-phase
27 clouds, however, only the Oruanui ash exhibited heterogeneous ice nucleation activity. Similar to
28 recent studies on mineral dust, we suggest that the mineralogy of volcanic ash may dictate its ice
29 nucleation activity in the immersion mode.

30 1 INTRODUCTION

31 It is estimated that approximately 9% of the world's population lives within 100 km of a
32 historically active volcano (Small and Naumann, 2001) and at any moment at least 20 volcanoes
33 around the globe may be erupting (Durant et al., 2010). In these areas, both gaseous and particulate
34 volcanic emissions can affect both human respiratory health (Horwell and Baxter, 2006) and local
35 environments (Witham et al., 2005). Further, explosive volcanic eruptions can greatly influence
36 global climate, even for years after the initial eruption (Durant et al., 2010). For example, the
37 eruption of Mt. Pinatubo in 1991 injected large amounts of gaseous sulfur species into the
38 stratosphere, which perturbed the climate system for 2-3 years following the eruption (Robock,
39 2004).

40 In addition to gaseous emissions, explosive volcanoes generate large amounts of fine ash (<
41 63 μm), which is dispersed into the atmosphere via plumes above volcanic vents and pyroclastic
42 flows. The global annual flux of fine volcanic ash into the atmosphere is approximately 200 Tg yr^{-1}
43 ¹, based on a 1000-yr average. While this flux is smaller than the terrestrial dust burden of
44 approximately 1000 to 4000 Tg yr^{-1} (Huneeus et al., 2011), volcanic eruptions are often sporadic
45 and can eject a large amount of particulate into the atmosphere over a short amount of time.
46 Furthermore, water vapor is abundant in volcanic eruptions, with up to 8% of the pre-eruptive
47 magma by mass (Durant et al., 2008). Thus, volcanic plumes represent prime conditions for ice
48 cloud glaciation via heterogeneous ice nucleation, yet this phenomenon is vastly understudied
49 considering its influence on plume dynamics, volcanic lightning, sequestration of gaseous species,
50 and the transport of these species to the stratosphere (Brown et al., 2012; McNutt and Williams,
51 2010; Kolb et al., 2010; Van Eaton et al., 2012). Further, fine ash from plumes can stay suspended
52 in the upper troposphere for weeks to months and travel 1000s of kilometers; if these particles are

53 efficient depositional ice nuclei, they could represent a widespread source of cold-cloud ice nuclei
54 not currently parameterized in global models (Hoose et al., 2010).

55 Active volcanoes have long been known to influence ice nuclei (IN) concentrations in the
56 atmosphere (Hobbs et al., 1971;Isono et al., 1959). For example, a study monitoring IN
57 concentrations in Japan found concentrations were enhanced by a factor of 40 over background
58 aerosol following the eruption of a nearby active volcano (Isono et al., 1959). In contrast, other
59 studies have shown that IN concentrations near volcanic plumes were not elevated above typical
60 background concentrations (Langer et al., 1974;Schnell and Delany, 1976). It was suggested,
61 however, that the ash in some of these studies had been deactivated by chemical processing via
62 gases in the volcanic cloud.

63 Laboratory studies probing the ice nucleation efficiency of volcanic ash have also shown it can
64 act as a heterogeneous IN (Durant et al., 2008;[Hoyle et al., 2011](#)). Unlike field measurements,
65 however, it has been suggested that all volcanic ash may have similar ice nucleation efficacy,
66 initiating ice formation in a relatively narrow temperature range of approximately 250 to 260 K
67 (Durant et al., 2008); however, these works are difficult to interpret quantitatively, especially in
68 cases where the nucleation mode is unclear, frozen fractions are unavailable, or the available
69 surface area has not been quantified. More recently, several studies have investigated the
70 deposition and/or immersion mode ice nucleation properties of ash from the 2010 eruption of the
71 Eyjafjallajökull volcano in Iceland (Steinke et al., 2011;Hoyle et al., 2011;Bingemer et al., 2012).
72 The results of these studies, combined with previous studies on large, 250-300 μm ash particles
73 from the 1980 Mt. St. Helens eruption (Fornea et al., 2009), suggests that there is one characteristic
74 ice nucleation efficiency for all ash, even when accounting for frozen fractions and surface area
75 (Murray et al., 2012). While such behavior would allow for a great simplification in models, these

76 results ~~represent~~ only ~~for~~ two volcanoes, ~~with similar classifications~~. Thus, the question still
77 remains of whether or not all volcanic ash exhibits similar ice nucleation activity regardless of the
78 location, pre-eruptive magma composition, and mineralogy.

79 In this study, we have collected volcanic ash particles from the Fuego (Guatemala),
80 Soufrière Hills (Montserrat), and Taupo (Oruanui eruption, New Zealand) volcanoes, which are
81 basaltic (45-52% SiO₂), andesitic (56-59% SiO₂), and rhyolitic ashes (63-75% SiO₂) (Heiken,
82 1972), respectively. These samples were specifically chosen to represent three separate
83 geographical locations, classifications by silica content, and percent minerals. For each of these
84 ashes, we have probed their depositional ice nucleation and immersion freezing potential. The
85 present experiment used to study depositional ice nucleation has been described previously;
86 however, this paper represents our first measurements of immersion freezing. For the depositional
87 nucleation experiments, the results are compared to previous results using the same system for the
88 clay mineral kaolinite (KGa-1b, Sihvonen et al., 2014), which is generally thought to be an
89 efficient depositional IN (Hoose and Moehler, 2012). For the immersion freezing experiments, the
90 Raman Microscope cold stage was validated using the same, standard kaolinite sample (Murray et
91 al., 2011;Pinti et al., 2012). Using this validated system, we determined the ice nucleation active
92 surface site densities of each volcanic ash sample by utilizing the singular description (Vali, 1994,
93 2008;Vali and Stansbury, 1966). The results and implications of these findings for cloud glaciation
94 in volcanic plumes and the atmosphere are discussed.

95 **2 EXPERIMENTAL**

96 **2.1 Volcanic Ash and Standard Minerals**

97 Volcanic ash was collected from three separate volcanic eruptions that produced three distinct
98 types of ash. Volcan Fuego (14.4828° N, 90.8828° W) is an active stratovolcano that lies 16 km

99 north of Antigua, Guatemala. The sub-Plinian eruption of October 14, 1974 produced ash fall that
100 impacted an area of $\sim 400 \text{ km}^2$, and samples used here were collected by previous researchers
101 immediately after eruption from a location 10 km from the vent. -The Soufrière Hills volcano
102 (16.7167° N, 62.1833° W) is an active stratovolcano located in Montserrat, an island in the Lesser
103 Antilles island arc of the West Indies. The ongoing eruption, which began in 1995, produces cyclic
104 dome-building and explosive activity, with samples used here resulting from an explosion in
105 January of 2010-; samples were collected immediately after deposition < 3 km from the vent.
106 Finally, the Taupo caldera (38.8056° S, 175.9008° E) sits in the center of the North Island of New
107 Zealand. Samples used here were collected from air fall deposits of the Oruanui ultra-Plinian
108 eruption $\sim 26 \text{ ka}$. The samples were excavated 39 km from the vent 25.4 ka after the eruption.

109 Volcanic ash (pyroclasts $< 2 \text{ mm}$) dominantly consists of silica-rich volcanic glass and
110 crystalline minerals. The chemical composition of volcanic ash is mainly determined from its
111 parent magma, although lithic material from the vent may play a role in modifying the composition
112 of the aerosolized ash. Since the main chemical elements of magma are Si and O, magma is often
113 classified by its silica content, which increases in the following order: basaltic (45-52% SiO_2),
114 andesitic (56-59% SiO_2), and rhyolitic (63-75% SiO_2) (Heiken, 1972). It is important to note that
115 silica content of the ash is determined from elemental analyses, most commonly as X-ray
116 fluorescence, and will include Si contributions from the melt glass, minerals, and lithic materials
117 in the ash; this is not to be confused with quartz, which can be one mineral component of the ash
118 composed is pure, crystalline SiO_2 . Each parent magma has a different melting temperature,
119 viscosity, and volatile content (dominantly H_2O); further, the assemblage and composition of
120 minerals often reflect their host melt (Langmann, 2014). The silica content and % crystals, taken
121 from previous whole-rock studies, for each of the volcanoes are shown in Table 1. As shown, the

122 Fuego, Soufrière Hills, and Oruanui whole-rock samples represent a range of magma compositions
123 and contain varying amounts of crystalline material. Chemical differences due to collection
124 distances from the vent or environmental aging were not explicitly taken into account in this study.
125 From these bulk studies, the primary mineral for all three samples was found to be plagioclase, a
126 tetrasilicate material in the feldspar family; however the samples vary in their next abundant
127 mineral. For the Fuego, Soufrière Hills, and Oruanui samples, the second-most abundant mineral
128 is olivine, amphibole, and quartz, respectively.

129 A low-defect kaolinite from Washington County, GA, USA (KGa-1b) was obtained from the
130 Source Clays Repository of the Clay Mineral Society (West Lafayette, IN, USA). KGa-1b was
131 chosen because it has been previously been studied in the ice nucleation literature in both the
132 deposition and immersion mode (Hoose and Moehler, 2012; Murray et al., 2012). Soda feldspar
133 [Standard Reference Material (SRM) 99b], a standard Na/Ca-feldspar, was obtained from the
134 National Institute of Standards and Technology (NIST) as a homogenous, fine powder (< 60 µm).

135 **2.2 Raman Microscope and Environmental Cell**

136 The Raman microscope has been described previously in detail (Baustian et al., 2010; Schill
137 and Tolbert, 2013). Briefly, a Nicolet Almega XR Raman spectrometer has been coupled to a
138 research grade Olympus BX-51 microscope with 10x, 20x, 50x, and 100x magnification
139 objectives. This Raman microscope has been outfitted with a Linkam THMS600 environmental
140 cell. The temperature of a cold stage inside the cell is controlled by a Linkam TMS94 automated
141 temperature controller with an accuracy of 0.1 K. Water partial pressure inside the cell is controlled
142 by mixing dry and humidified flows of N₂ and measured using a Buck Research CR-A1 dew point
143 hygrometer in line with the cell. The accuracy of the dew point hygrometer is 0.15 K. The relative
144 humidity (RH) and ice saturation ratio ($S_{\text{ice}} = P_{\text{H}_2\text{O}}/VP_{\text{ice}}$) inside the cell are determined by ratioing

145 the partial pressure of water to the equilibrium vapor pressure of water and ice, respectively
146 (Murphy and Koop, 2005). A Gast diaphragm pump at the exit of the hygrometer ensures that the
147 gas flow through the cell and hygrometer is 1 L min^{-1} .

148 Stokes-mode Raman spectra were obtained using a 532 nm frequency-doubled Nd:YAG as the
149 excitation laser. Spectra were taken from 200 to 4000 cm^{-1} with a typical resolution of $2\text{-}4 \text{ cm}^{-1}$.
150 Spectra were taken at the center of each particle and typically consisted of 256 co-added scans and
151 were taken with 50x and 100x long-range objectives, which focus the laser to a spot size of
152 approximately 1.3 and $1.1 \text{ }\mu\text{m}$, respectively (Everall, 2010). .

153 **2.3 Depositional Freezing**

154 For depositional freezing experiments, approximately 100 mg of ash was ground in a porcelain
155 mortar and pestle. To the ground ash, 8.0 mL of ultra-pure water was added and the slurry was
156 immediately aspirated into a Meinhard TR-50 glass concentric nebulizer. Nebulized droplets were
157 directed at a fused-silica disc and allowed to coagulate into supermicron droplets. The sample disc
158 was then transferred into the environmental cell and exposed to a low humidity environment. This
159 caused water evaporation, resulting in aggregated ash particles ranging from 1 to $20 \text{ }\mu\text{m}$ in lateral
160 diameter. Similar composite or aggregate volcanic ash samples are often found in the atmosphere,
161 and are produced by a similar mechanism (Brown et al., 2012). To assure that minimal chemical
162 alteration occurred from grinding and nebulizing the ash samples, Raman spectra of unground,
163 ground, and ground/nebulized and dried ash were obtained. An example set of these spectra for
164 Soufrière Hills ash is shown in Fig. 1. It can be seen that the main ash signatures at 507 cm^{-1} , 408
165 cm^{-1} , and 281 cm^{-1} in the Raman spectra are not significantly altered between the unground,
166 ground, and aggregated particles, indicating that any major chemical alteration due to ash
167 processing was not detected for these samples. A small peak at 663 cm^{-1} , however, does appear in

168 the ground and ground/nebulized and dried ash; we attribute this peak this better homogeneity of
169 minor components within the ground samples as compared to the unground samples.

170 Depositional nucleation experiments were conducted from 225-235 K. Experiments consisted
171 of increasing ice supersaturation over the sample by holding a constant vapor pressure of water
172 and lowering the temperature until the first ice event was noted. Specifically, after the particles
173 were allowed to sit at 298 K and ~0% RH for at least 10 minutes, the temperature was decreased
174 at a rate of 10 K min⁻¹, until $S_{ice} \sim 0.9$. The temperature was then decreased at a rate of 0.1 K min⁻¹,
175 which corresponds to an S_{ice} ramp rate of 0.01 min⁻¹, until the first ice event was noted. Initial
176 observation of ice was monitored by scanning the entire disc using the 10x objective. After the
177 first ice particle was detected, the 50x objective was utilized to verify the existence of ice both
178 visually (Fig. 2a) and spectrally. Finally, the ice was sublimed by turning off the flow of the
179 humidified nitrogen to ensure that ice had formed on an ash particle instead of the fused silica disc
180 (Fig. 2b). We have previously reported the conditions under which a blank fused-silica disc
181 initiates ice formation (Baustian et al., 2010). In that study, we found that the blank substrate
182 nucleated ice at S_{ice} of 1.6 to 2.33 from ~235 to 215 K.

183 **2.4 Immersion Freezing Experiments**

184 For immersion freezing experiments, it was important to ensure that the concentration of
185 volcanic ash or standard mineral in each drop was the same. Grinding with a mortar and pestle
186 produced samples too coarse to meet these requirements. Thus, for immersion freezing
187 experiments, a Wig-L-Bug® amalgamator (Crescent/Rinn Dental Mfg.) was used to pulverize
188 volcanic ash or standard minerals (Hudson et al., 2008; Curtis et al., 2008). Specifically,
189 approximately 100 mg of material was placed in a hardened stainless steel vial containing a
190 stainless steel ball pestle. The samples were pulverized in four five-minute intervals, for a total of

191 twenty minutes. The samples were allowed to rest for five-minutes between intervals to avoid
192 overheating of the sample. After treatment with the Wig-L-Bug®, the samples were made into 0.5,
193 1.0, and/or 2.0 wt% solutions with ultra-pure water. The concentration of material in suspensions
194 was determined gravimetrically. Sample solutions were shaken for at least 12 h prior to ice
195 nucleation experiments; this prevented unnecessary aggregation, and, therefore, ensured better
196 homogeneity between droplets. To generate droplets for an immersion freezing experiment, a
197 known weight-percent solution was aspirated into a Meinhard TR-30 glass concentric nebulizer.
198 To mitigate gravimetric settling prior to nebulization, humidified nitrogen was vigorously bubbled
199 through the sample solutions immediately before aspiration. Humidified N₂ was used as the carrier
200 gas to prevent excess evaporation at the nebulizer nozzle (Todoli and Mermet, 2011). The
201 nebulized spray was directed at a hydrophobically treated fused-silica disc, and the nebulized
202 droplets were allowed to coagulate into supermicron droplets. After nebulization, the disc was
203 immediately capped with an indium spacer (Alfa Aesar, 127 µm thick) and a second ~~quartz-fused-~~
204 silica disc. The spacer was coated with Apiezon L high-vacuum grease to ensure good contact to
205 the discs, which helped maintain a saturated humidity in the space created by the indium spacer
206 (immersion cell). By taking the above precautions, the concentration of ash in each particle is
207 assumed to be the same as the concentration of ash in the nebulized solution. To confirm this,
208 droplets were examined under 50x magnification prior to each experiment to ensure that their ash
209 concentrations were visually similar. Despite low relative humidities inside the environmental cell,
210 droplets inside the immersion cell did not visibly grow or shrink, even after sitting for 12 h.

211 Freezing experiments were video recorded under 10x or 20x magnification at 30 frames per
212 second, and freezing events were identified by the sudden appearance of structure within droplets.
213 Droplets were cooled from approximately 5 °C to -40 °C at a rate of 10 K min⁻¹. An example of

214 droplets at the beginning of an immersion freezing experiment prior to freezing and the same
215 droplets after all had frozen can be seen in Fig. 3a and 3b, respectively. Ice nucleation frozen
216 fractions were calculated as a function of temperature. Frozen fraction curves were separated into
217 two different size bins: 10-60 and 65-165 μm (droplet size, lateral diameter). These size bins span
218 droplet volumes from ~ 1.3 pL to 0.7 nL. In some cases, larger ice particles would grow at the
219 expense of smaller droplets in the cell. If these smaller droplets completely evaporated by the end
220 of the experiment, they were disregarded in our analysis. Further, by recording 30 frame-per-
221 second video, we could unambiguously determine if droplets coagulated or froze by contact
222 freezing. In all experiments, no contact-freezing events occurred from the contact of two liquid
223 drops. If two droplets coagulated, only their coagulated droplet size was considered. if unfrozen
224 Unfrozen droplets, however, could be ~~were~~ frozen by contact ~~frozen by~~ with growing ice particles;
225 those contact-frozen droplets were ~~also~~ disregarded in our analysis. Errors in n_s values are based
226 on the range of surface areas available in each experiment. The temperature error of 0.5 K for all
227 droplets, ~~0.5 K~~, was determined by repeated homogeneous freezing experiments ~~on~~ of ultra-pure
228 water.

229 **2.5 Brunaur-Emmet-Teller Surface Areas**

230 Brunaur-Emmet-Teller (BET) surface area analysis was conducted by Pacific Surface Sciences
231 Inc. using a Micrometric TriStarr II surface area analyzer. For BET analysis, ash samples and
232 Na/Ca-feldspar were prepared exactly as for immersion freezing experiments, but were not
233 suspended in high-purity water. The samples were degassed under flowing ultra-high purity grade
234 nitrogen for two hours at a temperature of 200 $^{\circ}\text{C}$ and the surface area was measured. Nitrogen
235 gas adsorption measurements were taken at relative pressures of 0.05, 0.1, 0.15, 0.2, and 0.25. The
236 free space in the analysis tube was measured by the Helium method. The five pressure points were

237 used to calculate the BET surface area. In this study, we determined the BET surface areas for all
238 three volcanic ash samples and Na/Ca-feldspar (Table 1).

239 **2.6 X-Ray Diffraction Analysis**

240 X-Ray Diffraction (XRD) analysis of volcanic ash and Na/Ca-feldspar was conducted by X-
241 Ray Wizards, LLC. Similar to BET analysis, each sample was prepared exactly as for immersion
242 freezing, but was not suspended into solution. Data was collected with a Bruker D8 Discover
243 instrument with a scintillation detector, Cu radiation, and appropriate slits for high resolution.
244 Percent crystallinity and associated % amorphous were determined by profile fitting and Degree
245 of Crystallinity measurements using the Bruker Rietveld Refinement (Table 1). Phase
246 identification and quantitative analysis were used to determine the identity and relative amount of
247 each phase in a mixture, and each identified mineral is reported as a wt% (Table 2). The
248 quantitative analysis was done via reference intensity ratio.

249 **3 RESULTS AND DISCUSSION**

250 **3.1 Depositional Ice Nucleation on Volcanic Ash Samples**

251 Depositional ice nucleation experiments using the Raman microscope have previously been
252 validated (Baustian et al., 2010; Wise et al., 2010). The critical S_{ice} needed for the onset of
253 depositional ice nucleation on all three ash samples from 225-235 K is shown in Fig. 4. It can be
254 seen that all three ash samples exhibit minimal temperature dependence and similar ice nucleation
255 activity to each other at the temperatures explored. Further, all three ash samples require low ice
256 supersaturations ($S_{ice} = 1.05 \pm 0.01$) to nucleate ice and, therefore, are efficient ice nuclei in the
257 temperature range investigated. Also shown in Fig. 4 are onset results from depositional ice
258 nucleation experiments on ash from the 2010 Eyjafjallajökull eruption from Hoyle et al. (2011)
259 and Steinke et al. (2011). Here, even the Icelandic ash has similar ice nucleation activity to the

260 three types of ash used in this study. To further highlight their depositional ice nucleation
261 efficiency, a parameterization of the critical ice saturation ratio of kaolinite from a previous study
262 (Sihvonen et al., 2014) has also been added to Fig. 4. Since these results were taken with the same
263 instrument for similar frozen fractions and surface areas, these results are directly comparable.
264 Thus, these results suggest it is possible that all volcanic ash studied to date are as efficient as clay
265 minerals for ice nucleation in the depositional mode.

266 To attempt to elucidate why these ash samples had similar, efficient depositional ice nucleation
267 abilities, we compared the % crystallinity and mineralogy for each ash. In Table 1, it can be seen
268 that the % crystallinity from our XRD results and the % crystals from the literature can be different.
269 This indicates that finer ash-sized fractions may have different properties from representative
270 whole-rock samples; thus, in this study we will only consider the % crystallinity and mineralogy
271 that we directly determined by XRD analysis. By comparing Fig. 4 with Table 1, it can be seen
272 that the % crystallinity and % amorphous between ash samples are different, but the S_{ice} onsets are
273 similar. Therefore, the total amount of crystalline vs. amorphous material is likely not the sole
274 factor in determining depositional ice nucleation. Table 2 indicates the detectable crystalline
275 material and their abundances ($\pm 3\%$). As shown, each of the ash samples contains a considerable
276 amount of plagioclase, either albite, a sodium-rich Na/Ca feldspar, or anorthite, a calcium-rich
277 Na/Ca-feldspar. Feldspar minerals, both K-feldspar and Na/Ca-feldspar, have previously been
278 shown to be among the most efficient depositional ice nuclei, comparable to kaolinite, Arizona
279 Test Dust, and Mojave Desert Dust (Yakobi-Hancock et al., 2013). Thus, we suggest that Na/Ca-
280 feldspar could be dictating the ice nucleation behavior of volcanic ash. It is important to note that
281 the above discussion only interprets ice nucleation efficiency in terms of a chemical mechanism.
282 The alteration of physical active sites from mechanical grinding or wet generation could increase

283 depositional ice nucleation efficiency; however, our results were comparable to both studies on
284 the Eyjafjallajökull ash, which used dry sieving to size select samples and aerosolized using dry-
285 generation techniques (Steinke et al., 2011;Hoyle et al., 2011).

286 **3.2 Validation of Immersion Freezing Experiments with Kaolinite**

287 To validate our immersion freezing experiments, we have run test experiments on KGa-1b.
288 KGa-1b was chosen because its ice nucleation behavior has been well studied in the immersion
289 freezing mode using both cold stage and continuous flow instruments (Murray et al., 2011;Pinti et
290 al., 2012). Our results for freezing of 10-60 μm droplets containing 1 wt% KGa-1b are shown in
291 Fig. 5. In this experiment, the cumulative fraction of frozen droplets [FF(T)] was determined as a
292 function of temperature:

$$293 \quad FF(T) = \frac{n_{ice}(T)}{n}, \quad (1)$$

294 where $n_{ice}(T)$ is the total number of frozen droplets at temperature T and n is the total number of
295 frozen droplets at 233.6 K. Also shown are results for homogeneous freezing of 10-60 μm ultra-
296 pure water droplets from our experimental setup. As expected, the homogeneous freezing curve
297 rises steeply at ~ -37 °C. The droplets containing 1% kaolinite freeze at higher temperatures than
298 the homogeneous freezing curve; thus, the droplets must be freezing heterogeneously. Differences
299 in droplet size bins, ash concentration, and droplet contact angle with the substrate affect both the
300 surface area available for ice nucleation and the subsequent frozen fraction at each temperature.
301 This renders it difficult to directly compare these results to former freezing spectra using different
302 experimental setups. It has, however, been shown in the past that inter-instrumental comparisons
303 of mineral dust can be made by invoking the singular approximation (Vali, 1994, 2008;Broadley
304 et al., 2012;Niemand et al., 2012). Here, the time dependence of freezing events is considered to
305 be of secondary importance to the temperature dependence. In this vein, a simplified quantification

306 of the observed frozen fractions and temperature onsets can be made by the metric of ice nucleation
 307 active site (INAS) densities (n_s) (DeMott et al., 1994), which is defined as:

$$308 \quad n_s(T, S_{ice}) = -\frac{\ln[1-FF(T, S_{ice})]}{SA_{aerosol}}, \quad (2)$$

309 where $SA_{aerosol}$ is the average surface area per particle. Our n_s values for KGa-1b as a function of
 310 temperature, calculated under the singular description, can be found in Fig. 6a. For $SA_{aerosol}$, the
 311 BET specific surface area was used. The BET surface area for KGa-1b was assumed to be 11.8 m^2
 312 g^{-1} (Murray et al., 2011). Also shown in Fig. 6a is an n_s parameterization for KGa-1b from Murray
 313 et al. (2011), who used a cold stage to determine the immersion freezing potential of KGa-1b for
 314 0.2 to 1 wt% solutions using various cooling rates. Our results lie slightly under the Murray
 315 parameterization; however, in our analysis we have ignored the time dependence of freezing
 316 events. While this may be valid for complex samples with a distribution of ice active sites
 317 (Niemand et al., 2012), it has been shown that one must take into account the time dependence for
 318 a pure clay mineral like kaolinite (Murray et al., 2011). Despite this, our data analyzed under the
 319 singular approximation are only one order of magnitude off from the parameterization. To take
 320 into account the time dependence, we invoke the modified singular theory (Vali, 2008). Here, the
 321 n_s value is modified to represent a single cooling rate. The parameterization is as follows:

$$322 \quad n_s(T, S_{ice}) = -\frac{\ln[1-FF(T-\alpha, S_{ice})]}{SA_{aerosol}}, \quad (3)$$

323 where the variable α is an offset in temperature from a freezing spectrum recorded at a cooling rate
 324 of 1 K min^{-1} . This is related to the cooling rate (r) by the equation

$$325 \quad \alpha = \beta \log(|r|), \quad (4)$$

326 where β is an empirical parameter. Our same KGa-1b data parameterized using the modified
 327 singular description with $\beta = 2.01$ (Murray et al., 2011) can be found in Fig. 6b. Now our data is
 328 in excellent agreement with the Murray parameterization. Thus, for immersion freezing, we find

329 that the Raman Microscope cold stage setup can be used to inter-compare inherent immersion
330 freezing abilities of particle types to other instruments under the singular or modified singular
331 approximation. This ability of the Raman Microscope cold stage to determine the inherent
332 immersion freezing ability of NX-Illite nanopowder has also been verified (Hiranuma et al.,
333 20154).

334 **3.3 Immersion Freezing of Droplets Containing Volcanic Ash Samples**

335 The immersion freezing results from 0.5, 1.0, and 2.0 wt% Oruanui, Soufrière Hills, and Fuego
336 volcanic ash are shown in Fig. 7. The Oruanui ash samples serve as heterogeneous immersion
337 mode ice nuclei for all wt% explored (Fig. 7a). In general, increasing the wt% of ash in each
338 droplet increases the freezing temperature. This is expected as increasing the wt% of ash in each
339 droplet increases the total surface area available for heterogeneous ice nucleation for a similar-
340 sized droplet population. Although their freezing spectra have different shapes, the temperature at
341 which 50% of 1% Oruanui ash droplets were frozen ($FF_{0.5}$) coincides with the $FF_{0.5}$ of 1 % KGa-
342 1b, indicating that they may have similar immersion freezing abilities. Unlike the depositional
343 freezing results, the immersion freezing activity of the Soufrière Hills ash is not similar to the
344 Oruanui ash (Fig. 7b). In fact, the FF curve for 10-60 μm droplets containing 2 wt% Soufrière
345 Hills ash overlaps with the ultra-pure water curve, implying that these droplets froze
346 homogeneously. Increasing the droplet size range to 65-165 μm only produces a few special IN at
347 $T > -37\text{ }^\circ\text{C}$; however, most droplet freezing events still coincide with the homogeneous freezing
348 curve. For 65-165 μm droplets containing 2 wt% Soufrière Hills ash, the total available surface
349 areas correlate to ash particles with spherical equivalent diameters of 23.0-53.6 μm , which forms
350 a large subset of fine volcanic ash. The Fuego ash has similar immersion freezing behavior to the
351 Soufrière Hills ash, despite coming from a different region and having different silica content (Fig.

352 7c). Again, for 10-60 μm droplets containing 2 wt% Fuego ash, the FF curve coincides with the
353 homogeneous freezing FF spectrum. Further, for 65-165 μm droplets containing 2 wt% Fuego ash,
354 whose total available surface area corresponded to ash particles 23.4 and 58.0 μm in spherical
355 diameter, only a few special IN at $T > -37\text{ }^\circ\text{C}$ are found.

356 Since these ash samples contain different wt% ash, droplet size populations, and ashes with
357 different surface areas, it is difficult to directly compare inherent ice nucleation activity from the
358 freezing spectra. Thus, we have calculated the n_s values for these ash samples under the singular
359 approximation (Fig. 8). For each ash, the BET specific surface area was used as determined in this
360 study (Table 1). The modified singular approximation was not used because larger particle-to-
361 particle variability of ice active sites is expected for these complex samples, limiting the
362 importance of time dependence (Broadley et al., 2012; Hiranuma et al., 2015⁴). As shown in Fig.
363 8, the Oruanui ash is inherently a better ice nuclei than either the Soufrière Hills or Fuego Ash,
364 which are similar to each other. Also shown in Fig. 8 are n_s values of Mt. St. Helens and
365 Eyjafjallajökull ash from previous studies (Hoyle et al., 2011; Steinke et al., 2011; Murray et al.,
366 2012). The Oruanui ash sits below these points; however it should be noted that the surface area
367 of the Eyjafjallajökull and Mt. St. Helens ash were estimated using their geometrical surface area.
368 Due to the high degree of aggregation and porosity of volcanic ash particles, the geometrical
369 surface area could be vastly underestimating the true surface area. To estimate this effect, we have
370 re-plotted the volcanic ash parameterization found in Murray et al. (2012), assuming that the true
371 surface area is 10 times greater than the estimated geometrical surface area. This is not an
372 unreasonable assumption, since the geometrical surface area would underestimate the true surface
373 area 4-20 times for ash particles 1-5 μm in diameter, assuming a BET surface area for Oruanui ash
374 and a density of 2.6 g m^{-3} . The adjusted parameterization is shown in Fig. 8 as a dashed line. As

375 shown, estimating the surface area as 10 times greater than the geometrical surface area brings the
376 parameterization much closer to our results. Thus, although the Oruanui ash has different surface-
377 area normalized ice nucleation abilities than the Fuego and Soufrière Hills ash used in this study,
378 it appears to be similar to the Eyjafjallajökull and Mt. St. Helens ash.

379 **3.4 Immersion Freezing of Droplets Containing Na/Ca Feldspar**

380 Recently, it has been shown that K-feldspar is an extremely efficient ice nucleus and,
381 consequently, may dictate the ice nucleation ability of natural mineral dust, even though it is only
382 found in low weight percentages (Atkinson et al., 2013). That study also determined the ice
383 nucleation ability of Na/Ca-feldspar from the Bureau of Analysed Samples (United Kingdom), and
384 found that it was also an efficient immersion ice nucleus. In our results, we found that neither the
385 Fuego nor Soufrière Hills ash acted as efficient immersion freezing ice nuclei for the
386 concentrations and droplet sizes that we explored. While the Fuego and Soufrière Hills ash both
387 contained significant feldspar, it was almost exclusively the Na/Ca-feldspar. To explore this
388 further, we conducted immersion freezing experiments on NIST SRM 99b, a Na/Ca-feldspar
389 standard. We also conducted XRD on these samples, and found that they contained K-feldspar and
390 quartz impurities in addition to Na/Ca-Feldspar (Table 2). The frozen fraction curves for NIST
391 SRM 99b are plotted in Fig. 9 and their n_s values are shown in Fig. 8. As shown, the NIST SRM
392 99b is also an efficient ice nucleus. We suggest that the high immersion freezing activity of the
393 NIST 99b soda feldspar is due to the K-feldspar impurities, in agreement with previous studies
394 (Atkinson et al., 2013). ~~To our knowledge, a laboratory standard of Na/Ca-feldspar cannot be~~
395 ~~obtained without these K-feldspar impurities.~~ These combined results suggest that Na/Ca-feldspar
396 may be inactive in the immersion mode despite being very active for depositional nucleation. This
397 is in agreement with Zolles et al. (2015), who found that the Na/Ca-feldspars albite, anorthian

398 andesine, and an albite-dominated ash sample were all weak immersion-mode IN. Thus, from
399 examining Table 2, we suggest that the immersion freezing activity of the Oruanui ash is likely
400 due to the quartz. This is in agreement with previous findings, who found that quartz was the
401 second-most efficient immersion mode nuclei mineral found in mineral dust behind feldspars
402 (Atkinson et al., 2013).

403 It is important to note that the above discussion interprets immersion freezing only from a
404 chemical mechanism standpoint. The ash samples used here were collected at various distances
405 from the volcano and represent various magnitudes of eruption explosivity, which affects grain
406 morphology and the grain size distribution of the fall deposit, however, it is important to note that
407 these samples were processed prior to immersion freezing. Namely, even after size sorting, the
408 particles were pulverized from larger ash particles and immersed in water and shaken for at least
409 12 h prior to immersion freezing experiments. Pulverizing the ash particles has two possible effects
410 on ice nucleation. First, it could introduce new, physical active sites. For example it has been
411 shown for hematite particles that mechanical milling can change the ice nucleation surface site
412 density, even when accounting for changes in surface area (Hiranuma et al., 2014). Second, it
413 could liberate and/or expose mineral surfaces that were previously encased in volcanic glass. Both
414 of these effects, however, are expected to increase ice nucleation activity and do not account for
415 the inactivity of the Fuego and Soufrière Hills ashes in the immersion mode. Further, in some
416 cases, approximately 70% of fine ash particles (< 63 μm) are largely aggregates of smaller particles
417 (Brown et al., 2012). Thus, pulverizing with the Wig-L-Bug® amalgamator may only break apart
418 these aggregates. In the past, it has been shown that wet generation techniques can affect the
419 hygroscopicity and cloud droplet formation ability of mineral dust (Sullivan et al., 2010; Garimella
420 et al., 2014). Thus, allowing the ash samples to shake in solution for at least 12 h prior to immersion

421 freezing experiments could cause the dissolution/redistribution of active surface sites. This,
422 however, is unlikely since this treatment was also conducted for kaolinite, which agrees with
423 previous literature values of wet and dry generated KGa-1b (Pinti et al., 2012; Murray et al., 2011).

424 **4 ATMOSPHERIC IMPLICATIONS**

425 Previously, it has been suggested that all volcanic ash has similar ice nucleation efficiency and
426 may initiate ice below 250-260 K, leading to an overseeding of ice in volcanic plumes (Durant et
427 al., 2008). Since volcanic ash concentration in plumes can be up to 1000 cm^{-3} , overseeding of ice
428 could create a dearth of supercooled water droplets and shut down the Bergeon-Findeisen process,
429 the process of ice crystal growth at the expense of supercooled liquid droplets in mixed-phase
430 clouds. Thus, since particle growth would be reliant on collision processes, overseeding could
431 retard or even prevent the development of precipitation in volcanic plumes. In this work, we have
432 shown that three distinct types of volcanic ash have similar, efficient ice nucleation onsets in the
433 deposition mode. It has been suggested that, large amounts of water in pre-eruptive magma (up to
434 8% by mass) may render concentration of water in volcanic plumes greater than for typical
435 thunderstorms (McNutt and Williams, 2010). Thus, the primary mode of ice nucleation in volcanic
436 plumes may be immersion freezing. Unlike depositional freezing, the volcanic ash in this study
437 did not possess the same ice nucleation efficiency in the immersion mode; indeed, both the Fuego
438 and Soufrière Hills ash seem inactive in the immersion mode for droplets containing a surface area
439 of ash equivalent to a spherical ash particle $\sim 60 \mu\text{m}$ in diameter. Thus, our results indicate that
440 some volcanic plumes may not be overseeded with ice. Indeed, this has been directly observed in
441 some volcanic plumes such as the 17 September 1992 eruption of Mt Spurr, where remote sensing
442 measurements showed that ash mass dominated over ice mass (Rose et al., 2001). The current
443 study suggests that immersion freezing, and therefore overseeding, may be dictated by the

444 differences in the mineralogy of the crystalline material found in volcanic ash. Thus, the
445 identification and quantification of mineral phases in fine volcanic ash may be important to
446 correctly predict the many processes in volcanic plumes that rely on ice and hydrometeor
447 formation.

448 It has been shown that ash aggregation, which controls volcanic cloud dispersal, may be reliant
449 on hydrometeor formation (Rose and Durant, 2011). If a volcanic plume is overseeded with ice,
450 hydrometeor growth will be retarded, reducing aggregation and prolonging the lifetime and
451 dispersal of the volcanic cloud (Brown et al., 2012). Correctly modeling volcanic cloud lifetimes
452 and dispersal has important implications for both human health and aviation traffic. Volcanic
453 lightning is another understudied process in volcanic plumes that is thought to be influenced by
454 ice formation (McNutt and Williams, 2010). Volcanic lightning in high-altitude plumes is thought
455 to be produced along a similar mechanism to thundercloud electrification and is important because
456 it represents a hazard and contributes to the global electrification circuit. From this work, we show
457 that some types of ash, depending on their mineralogy, may not initiate ice until the homogeneous
458 freezing limit. Thus, previous thresholds of ice formation in volcanic plumes of 250-260 K may
459 be overestimating the amount of volcanic lightning predicted in models.

460 Volcanic ash also has important climatic implications beyond the initial plume. Fine volcanic
461 ash can stay suspended in the atmosphere for 24 hours and travel 100s to 1000s of km (Brown et
462 al., 2012). Previous work has shown that, while initial plumes contain large concentrations of
463 water, volcanic clouds can dry out markedly within hours of entering the atmosphere (Schultz et
464 al., 2006). Further, very fine ash can stay suspended much longer than 24 hours and ash fall
465 deposits may remain in local environments for years to decades and can be re-suspended due to
466 human activity (Horwell and Baxter, 2006). In this work, we have shown that all three samples of

467 volcanic ash had similar depositional ice nucleation efficiency ($S_{\text{ice}} = 1.05 \pm 0.01$), likely due to
468 Na/Ca-feldspars, which is similar to previous findings on proxies of mineral dust. Thus, since
469 depositional nucleation can occur at lower temperatures than immersion freezing, fine volcanic
470 ash represents a potentially important source of global cold-cloud ice nuclei. Indeed, in one study
471 that took daily measurements of IN concentrations over a 2-year period from central Germany, the
472 highest IN concentrations ever recorded coincided with backwards trajectories of the
473 Eyjafjallajökull volcanic eruption in Iceland (Bingemer et al., 2012). In that same study, the IN
474 concentrations in Israel, over 5000 km away from the source of the eruption, were determined for
475 air-masses originated from the same volcanic eruption. The high IN concentrations found in those
476 air masses were rivaled only during desert dust storms. Electron microscopy measurements
477 confirmed that the most abundant IN in these air masses were volcanic ash. Furthermore, a study
478 using polarization lidars at two central-European stations found a clear influence of volcanic ash
479 on heterogeneous ice nucleation of tropospheric clouds. For example, in that study, all observed
480 cloud layers with cloud top temperatures < -15 C contained ice during the days following the April
481 2010 Eyjafjallajökull volcanic eruption (Seifert et al., 2011).

482 Our experimental results suggest that ice nucleation on fine volcanic ash may exert a non-
483 negligible effect on volcanic plume lifetimes and dynamics as well as on global climate through
484 the formation of cirrus clouds; however, volcanic ice nuclei are currently neglected in global
485 climate models (Hoose et al., 2010). While previous works indicate that a simple parameterization
486 for all ash types may be possible for the simplification of parameterizing immersion mode volcanic
487 ash ice nuclei in models (Murray et al., 2012), our results indicate that ash types could differ in ice
488 nucleation properties, likely due to their mineralogy. Depositional nucleation on volcanic ash,
489 however, may fall under such a parameterization since all three, distinct ash samples displayed

490 similar depositional ice nucleation onsets to each other and to previous studies on ash from the
491 Eyjafjallajökull volcano (Steinke et al., 2011;Hoyle et al., 2011).

492 **ACKNOWLEDGEMENTS**

493 This work was supported by the National Science Foundation under grants AGS1048536. We
494 thank Bill Rose, Alexa Van Eaton, and the Montserrat Volcano Observatory for the utilized ash
495 samples.

496

Table 1. Silica content, % crystals from previous whole-rock studies, XRD % crystallinity and % amorphous, and the BET surface areas of representative volcanic rock and ash samples from the Fuego, Soufrière Hills, and Taupo volcanoes and powdered NIST SRM-99b Na/Ca-Feldspar.

Sample	Silica Content (wt%)	% Crystals	XRD % Crystallinity	XRD % Amorphous	BET Surface Area (m ² g ⁻¹)
Fuego (Guatemala)	50.6 ^a	38 vol% ^a	63 ± 3	37	5.14 ± 0.03
Soufrière Hills (Montserrat)	59.13 ^b	60-87 wt% ^b	89 ± 3	11	6.30 ± 0.04
Taupo (Oruanui, New Zealand)	74.15 ^c	3-13 wt% ^c	41 ± 3	59	9.23 ± 0.04
Na/Ca-Feldspar (NIST)	-	-	100 ± 3	0	1.219 ± 0.008

^a(Rose et al., 1978)

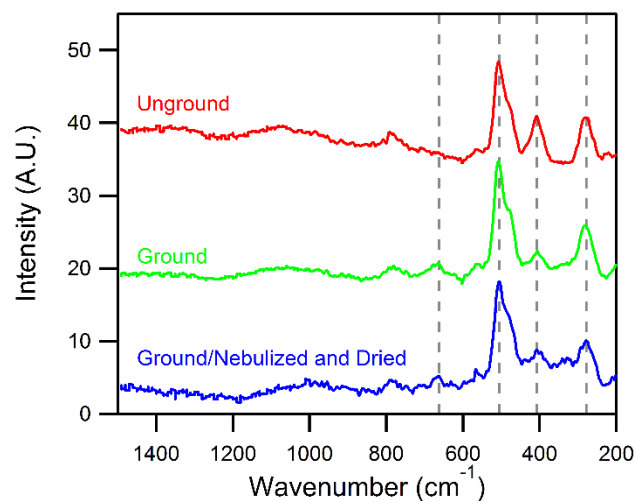
^b(Murphy et al., 2000)

^c(Wilson et al., 2006)

498 **Table 2.** The mineralogical composition of Fuego, Soufrière Hills, and Oruanui volcanic ash and
 499 NIST SRM-99b Na/Ca-feldspar as determined by XRD.

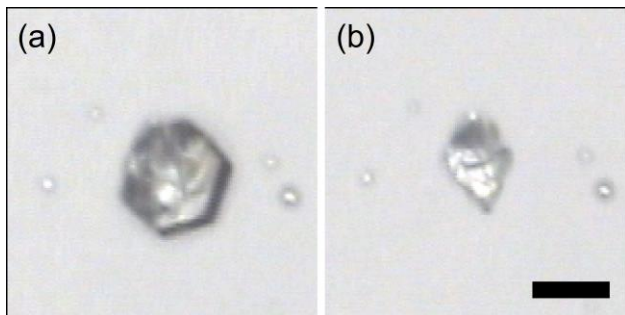
Mineral/Sample	Anorthite Ca/Na- Feldspar	Albite Na/Ca- Feldspar	Microcline K- Feldspar	Quartz SiO ₂	Enstatite Ortho- pyroxene	Riebeckite Magnesio- hornblende	Other (Trace)
Fuego	36	64	-	-	-	-	-
Soufrière Hills	10	71	-	1	11	7	-
Oruanui	26	47	-	27	-	-	-
Na/Ca-Feldspar (NIST)	-	69	18	13	-	-	Anorthite, Anorthoclase, Barium Silicate Hydrate

500



501

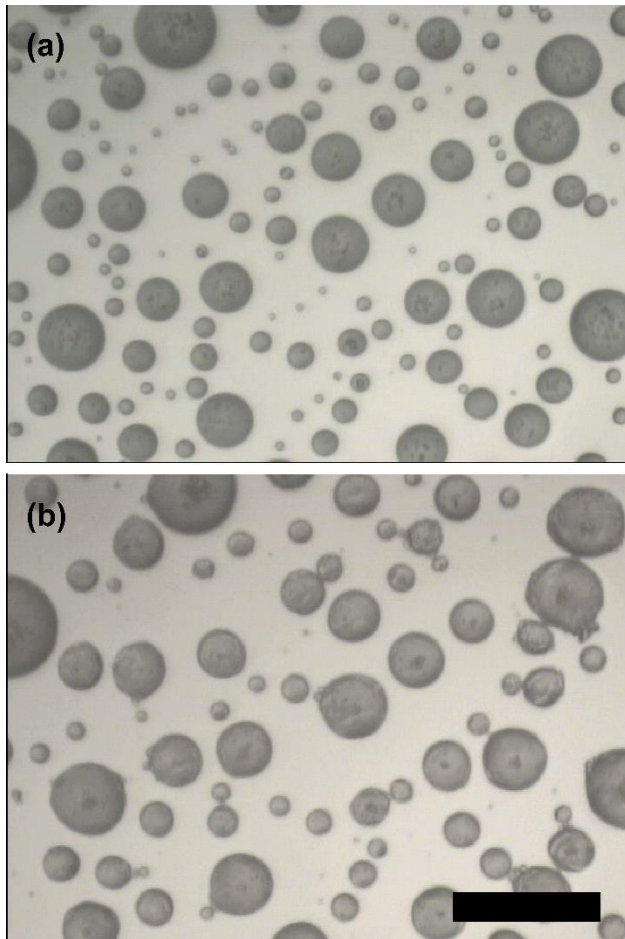
502 **Figure 1.** A set of example Raman spectra of unground, ground, and ground/nebulized Soufrière
 503 Hills volcanic ash. As shown, the main peaks at 507 cm⁻¹, 408 cm⁻¹, and 281 cm⁻¹ (vertical
 504 dashed lines) are minimally affected by mechanical grinding and wet generation, suggesting that
 505 bulk chemical alteration does not occur. A small peak at 663 cm⁻¹, however, does appear in the
 506 ground samples, possibly due to better homogeneity of minor components when compared to
 507 unground samples.



508

509 **Figure 2.** 50x optical image of an ice particle at 225 K (a) and its Fuego ash nucleus (b). The
510 scale bar in the bottom right-hand corner equals 10 μm .

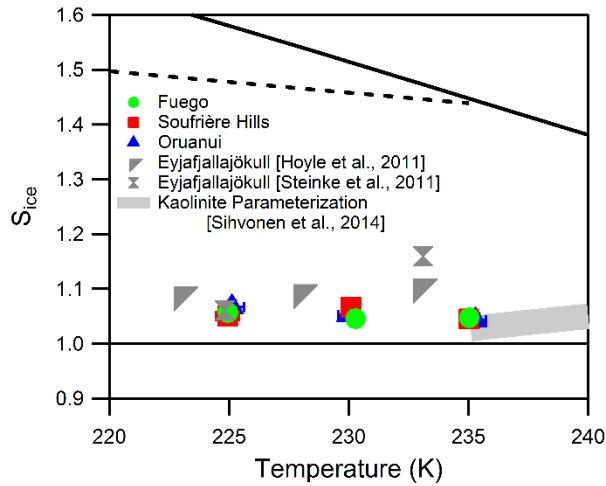
511



512

513 **Figure 3.** 20x images of unfrozen droplets containing 1% KGa-1b (a), and the same drops after
514 an immersion freezing experiment (b). The scale bar in the bottom right-hand corner equals 100
515 μm .

516



517

518 **Figure 4.** The onset S_{ice} as a function of temperature for nucleation on volcanic ash samples. The

519 thick and thin solid lines refer to water and ice saturation respectively. The dashed line represents

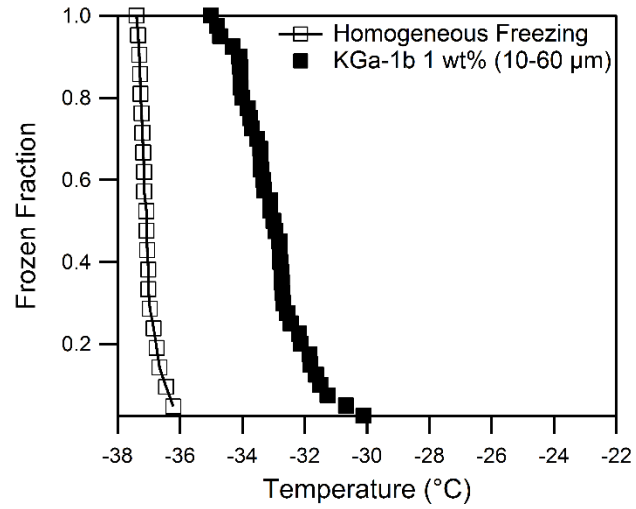
520 the S_{ice} values for homogeneous nucleation of an aqueous droplet (Koop et al., 2000). Also

521 included are onset results from depositional ice nucleation experiments on ash from the 2010

522 Eyjafjallajökull eruption (Hoyle et al., 2011;Steinke et al., 2011) and a parameterization for

523 depositional ice nucleation on KGa-1b (Sihvonen et al., 2014).

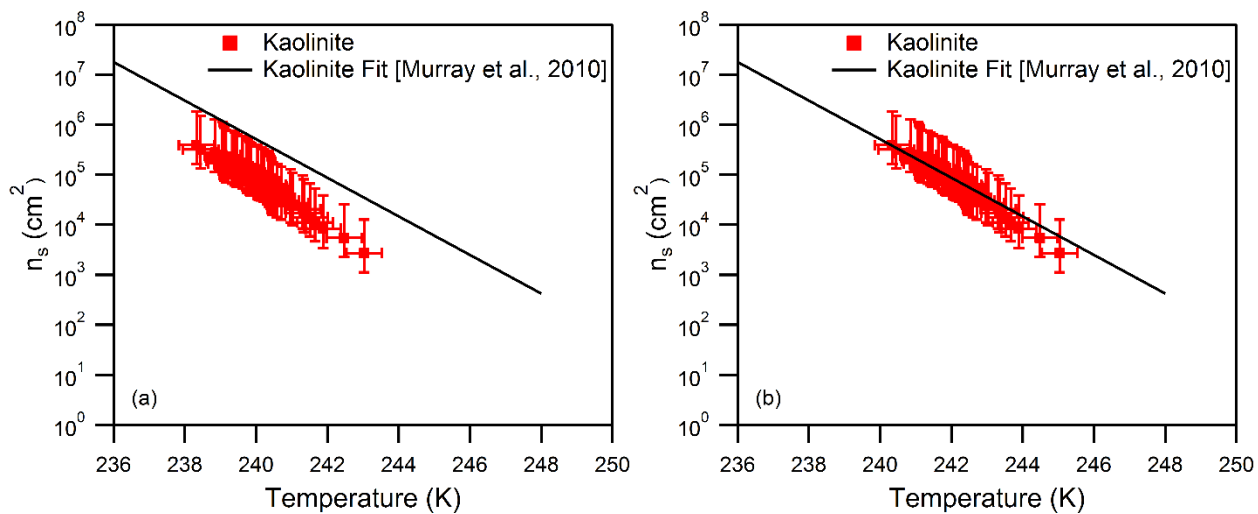
524



525

526 **Figure 5.** Frozen fraction curve for 1wt% KGa-1b in 10-60 μm droplets as a function of
527 temperature. Also shown are results for freezing of ultra-pure water droplets (homogeneous
528 freezing).

529

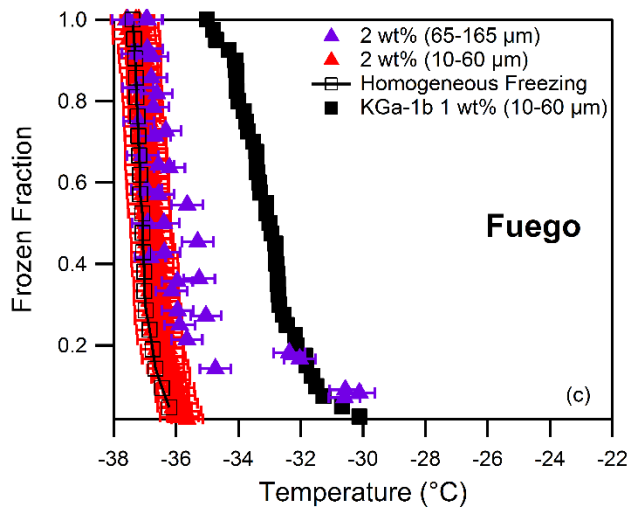
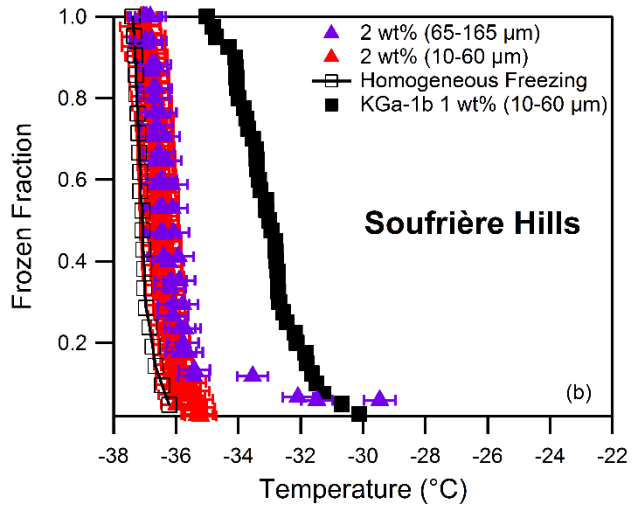
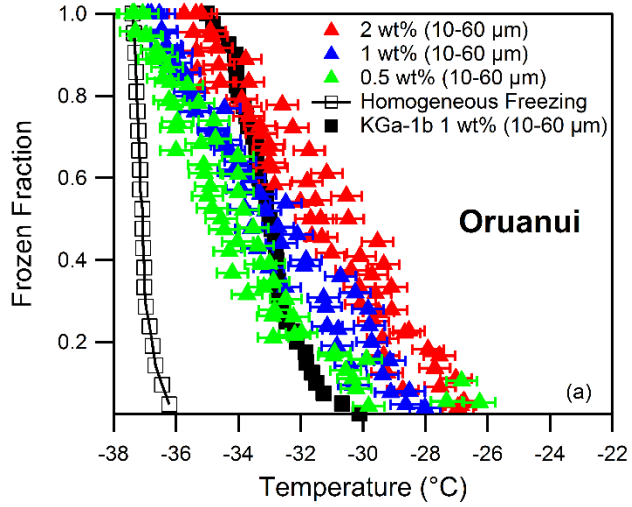


530

531 **Figure 6.** Ice nucleation active surface site densities for KGa-1b as a function of temperature using

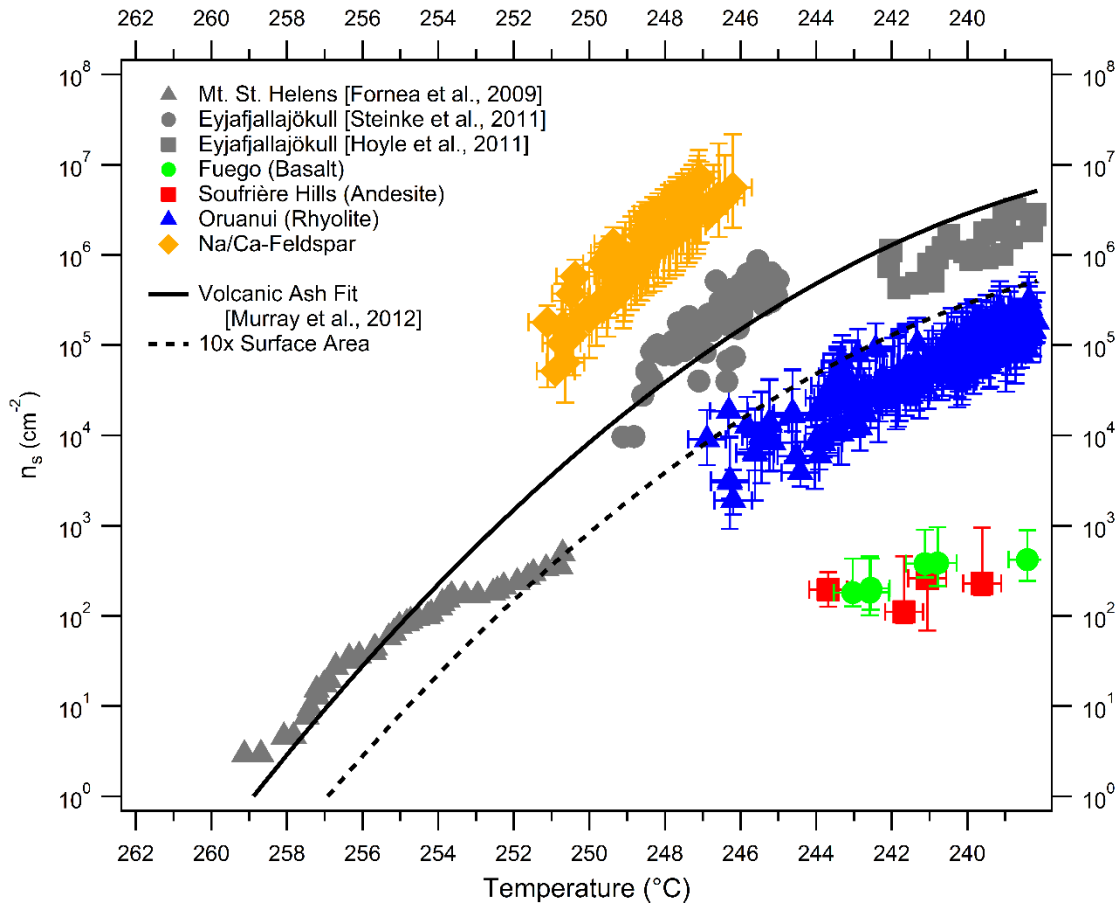
532 the singular description (a) and the modified singular description (b).

533



537 **Figure 7.** Frozen fraction curves as a function of temperature for 0.5, 1.0, and/or 2 wt% Oruanui
538 ash (a), Soufrière Hills (b), and Fuego Ash (c).

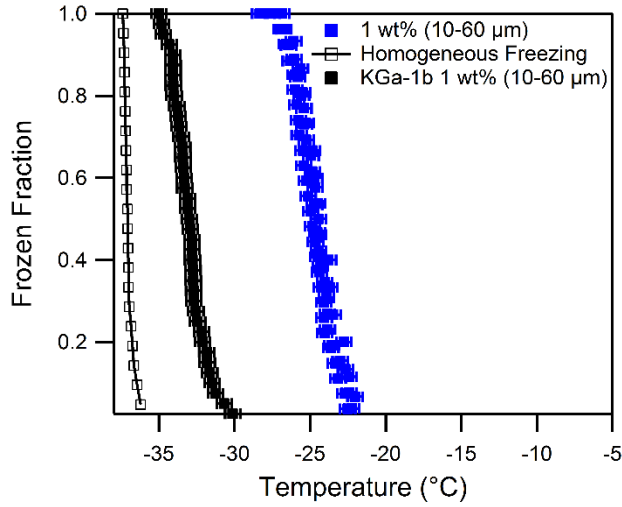
539



540

541 **Figure 8.** Ice nucleation active surface site densities as a function of temperature for Oruanui,
 542 Soufrière Hills, and Fuego ash and NIST SRM-99b Soda Feldspar. Also shown are n_s -values for
 543 previous studies (grey markers) on volcanic ash and a parameterization for that data (solid line,
 544 (Murray et al., 2012). Additionally, a new parameterization has also been shown that assumes
 545 surface area of the volcanic to be 10 times greater than the original parameterization to account for
 546 the high porosity of volcanic ash (dashed line).

547



548

549 **Figure 9.** Frozen fraction curve for 1 wt% Na/Ca Feldspar in 10-60 μm droplets as a function of
 550 temperature.

551

References

- 552
553
- 554 Atkinson, J. D., Murray, B. J., Woodhouse, M. T., Whale, T. F., Baustian, K. J., Carslaw,
555 K. S., Dobbie, S., O'Sullivan, D., and Malkin, T. L.: The importance of feldspar for ice nucleation
556 by mineral dust in mixed-phase clouds, *Nature*, 498, 355-358, doi:10.1038/nature12278, 2013.
- 557 Baustian, K. J., Wise, M. E., and Tolbert, M. A.: Depositional ice nucleation on solid
558 ammonium sulfate and glutaric acid particles, *Atmos. Chem. Phys.*, 10, 2307-2317,
559 doi:10.5194/acp-10-2307-2010, 2010.
- 560 Bingemer, H., Klein, H., Ebert, M., Haunold, W., Bundke, U., Herrmann, T., Kandler, K.,
561 Mueller-Ebert, D., Weinbruch, S., Judt, A., Weber, A., Nillius, B., Ardon-Dryer, K., Levin, Z.,
562 and Curtius, J.: Atmospheric ice nuclei in the Eyjafjallajokull volcanic ash plume, *Atmos. Chem.*
563 *Phys.*, 12, 857-867, doi:10.5194/acp-12-857-2012, 2012.
- 564 Broadley, S. L., Murray, B. J., Herbert, R. J., Atkinson, J. D., Dobbie, S., Malkin, T. L.,
565 Condliffe, E., and Neve, L.: Immersion mode heterogeneous ice nucleation by an illite rich powder
566 representative of atmospheric mineral dust, *Atmos. Chem. Phys.*, 12, 287-307, doi:10.5194/acp-
567 12-287-2012, 2012.
- 568 Brown, R. J., Bonadonna, C., and Durant, A. J.: A review of volcanic ash aggregation,
569 *Phys. Chem. Earth*, 45-46, 65-78, doi:10.1016/j.pce.2011.11.001, 2012.
- 570 Curtis, D. B., Meland, B., Aycibin, M., Arnold, N. P., Grassian, V. H., Young, M. A., and
571 Kleiber, P. D.: A laboratory investigation of light scattering from representative components of
572 mineral dust aerosol at a wavelength of 550 nm, *J. Geophys. Res.-Atmos.*, 113, D08210,
573 doi:10.1029/2007jd009387, 2008.
- 574 DeMott, P. J., Meyers, M. P., and Cotton, W. R.: Parameterization and impact of ice
575 initiation processes relevant to numerical-model simulations of cirrus clouds, *J. Atmos. Sci.*, 51,
576 77-90, doi:10.1175/1520-0469(1994)051<0077:paioii>2.0.co;2, 1994.
- 577 Durant, A. J., Shaw, R. A., Rose, W. I., Mi, Y., and Ernst, G. G. J.: Ice nucleation and
578 overseeding of ice in volcanic clouds, *J. Geophys. Res.-Atmos.*, 113, D09206,
579 doi:10.1029/2007jd009064, 2008.
- 580 Durant, A. J., Bonadonna, C., and Horwell, C. J.: Atmospheric and Environmental Impact
581 of Volcanic Particulates, *Elements*, 6, 235-240, doi:10.2113/gselements.6.4.235, 2010.
- 582 Overall, N. J.: Confocal Raman microscopy: common errors and artefacts, *Analyst*, 135,
583 2512-2522, doi:10.1039/c0an00371a, 2010.

584 Fornea, A. P., Brooks, S. D., Dooley, J. B., and Saha, A.: Heterogeneous freezing of ice on
585 atmospheric aerosols containing ash, soot, and soil, *J. Geophys. Res.-Atmos.*, 114,
586 doi:10.1029/2009jd011958, 2009.

587 Garimella, S., Huang, Y. W., Seewald, J. S., and Cziczo, D. J.: Cloud condensation nucleus
588 activity comparison of dry- and wet-generated mineral dust aerosol: the significance of soluble
589 material, *Atmos. Chem. Phys.*, 14, 6003-6019, doi:10.5194/acp-14-6003-2014, 2014.

590 Heiken, G.: Morphology and petrography of volcanic ashes, *Geological Society of
591 America Bulletin*, 83, 1961-1988, doi:10.1130/0016-7606(1972)83[1961:mapova]2.0.co;2, 1972.

592 Hiranuma, N., Hoffmann, N., Kiselev, A., Dreyer, A., Zhang, K., Kulkarni, G., Koop, T.,
593 and Moehler, O.: Influence of surface morphology on the immersion mode ice nucleation
594 efficiency of hematite particles, *Atmospheric Chemistry and Physics*, 14, 2315-2324,
595 doi:10.5194/acp-14-2315-2014, 2014.

596 [Hiranuma, N., Augustin-Bauditz, S., Bingemer, H., Budke, C., Curtius, J., Danielczok, A.,
597 Diehl, K., Dreischmeier, K., Ebert, M., Frank, F., Hoffmann, N., Kandler, K., Kiselev, A., Koop,
598 T., Leisner, T., Möhler, O., Nillius, B., Peckhaus, A., Rose, D., Weinbruch, S., Wex, H., Boose,
599 Y., DeMott, P. J., Hader, J. D., Hill, T. C. J., Kanji, Z. A., Kulkarni, G., Levin, E. J. T., McCluskey,
600 C. S., Murakami, M., Murray, B. J., Niedermeier, D., Petters, M. D., O'Sullivan, D., Saito, A.,
601 Schill, G. P., Tajiri, T., Tolbert, M. A., Welti, A., Whale, T. F., Wright, T. P., and Yamashita, K.:
602 A comprehensive laboratory study on the immersion freezing behavior of illite NX particles: a
603 comparison of 17 ice nucleation measurement techniques, *Atmos. Chem. Phys.*, 15, 2489-2518,
604 doi:10.5194/acp-15-2489-2015, 2015.](#)

605 Hobbs, P. V., Fullerton, C.M, and Bluhm, G. C.: ICE NUCLEUS STORMS IN HAWAII,
606 *Nat.-Phys. Sci.*, 230, 90-1, 1971.

607 Hoose, C., Kristjansson, J. E., Chen, J.-P., and Hazra, A.: A Classical-Theory-Based
608 Parameterization of Heterogeneous Ice Nucleation by Mineral Dust, Soot, and Biological Particles
609 in a Global Climate Model, *J. Atmos. Sci.*, 67, 2483-2503, doi:10.1175/2010jas3425.1, 2010.

610 Hoose, C., and Moehler, O.: Heterogeneous ice nucleation on atmospheric aerosols: a
611 review of results from laboratory experiments, *Atmos. Chem. Phys.*, 12, 9817-9854,
612 doi:10.5194/acp-12-9817-2012, 2012.

613 Horwell, C. J., and Baxter, P. J.: The respiratory health hazards of volcanic ash: a review
614 for volcanic risk mitigation, *B. Volcanol.*, 69, 1-24, doi:10.1007/s00445-006-0052-y, 2006.

615 Hoyle, C. R., Pinti, V., Welti, A., Zobrist, B., Marcolli, C., Luo, B., Hoeskuldsson, A.,
616 Mattsson, H. B., Stetzer, O., Thorsteinsson, T., Larsen, G., and Peter, T.: Ice nucleation properties
617 of volcanic ash from Eyjafjallajökull, *Atmos. Chem. Phys.*, 11, 9911-9926, doi:10.5194/acp-11-
618 9911-2011, 2011.

- 619 Hudson, P. K., Gibson, E. R., Young, M. A., Kleiber, P. D., and Grassian, V. H.: Coupled
620 infrared extinction and size distribution measurements for several clay components of mineral dust
621 aerosol, *J. Geophys. Res.-Atmos.*, 113, D011201, doi:10.1029/2007jd008791, 2008.
- 622 Huneeus, N., Schulz, M., Balkanski, Y., Griesfeller, J., Prospero, J., Kinne, S., Bauer, S.,
623 Boucher, O., Chin, M., Dentener, F., Diehl, T., Easter, R., Fillmore, D., Ghan, S., Ginoux, P.,
624 Grini, A., Horowitz, L., Koch, D., Krol, M. C., Landing, W., Liu, X., Mahowald, N., Miller, R.,
625 Morcrette, J. J., Myhre, G., Penner, J., Perlwitz, J., Stier, P., Takemura, T., and Zender, C. S.:
626 Global dust model intercomparison in AeroCom phase I, *Atmos. Chem. Phys.*, 11, 7781-7816,
627 doi:10.5194/acp-11-7781-2011, 2011.
- 628 Isono, K., Komabayasi, M., and Ono, A.: Volcanoes as a source of atmospheric ice nuclei,
629 *Nature*, 183, 317-318, doi:10.1038/183317a0, 1959.
- 630 Kolb, C. E., Cox, R. A., Abbatt, J. P. D., Ammann, M., Davis, E. J., Donaldson, D. J.,
631 Garrett, B. C., George, C., Griffiths, P. T., Hanson, D. R., Kulmala, M., McFiggans, G., Poschl,
632 U., Riipinen, I., Rossi, M. J., Rudich, Y., Wagner, P. E., Winkler, P. M., Worsnop, D. R., and O'
633 Dowd, C. D.: An overview of current issues in the uptake of atmospheric trace gases by aerosols
634 and clouds, *Atmos. Chem. Phys.*, 10, 10561-10605, doi:10.5194/acp-10-10561-2010, 2010.
- 635 Koop, T., Luo, B. P., Tsias, A., and Peter, T.: Water activity as the determinant for
636 homogeneous ice nucleation in aqueous solutions, *Nature*, 406, 611-614, 10.1038/35020537,
637 2000.
- 638 Langer, G., Garcia, C. J., Mendonca, B. G., Pueschel, R. F., and Fullerton, C.M.: Hawaiian
639 volcanos—source of ice nuclei, *J. Geophys. Res.*, 79, 873-875, doi:10.1029/JC079i006p00873,
640 1974.
- 641 Langmann, B.: On the Role of Climate Forcing by Volcanic Sulphate and Volcanic Ash,
642 *Adv. Meteorol.*, 340123, doi:10.1155/2014/340123, 2014.
- 643 McNutt, S. R., and Williams, E. R.: Volcanic lightning: global observations and constraints
644 on source mechanisms, *B. Volcanol.*, 72, 1153-1167, doi:10.1007/s00445-010-0393-4, 2010.
- 645 Murphy, D. M., and Koop, T.: Review of the vapour pressures of ice and supercooled water
646 for atmospheric applications, *Q. J. Roy. Meteorol. Soc.*, 131, 1539-1565, doi:10.1256/qj.04.94,
647 2005.
- 648 Murphy, M. D., Sparks, R. S. J., Barclay, J., Carroll, M. R., and Brewer, T. S.:
649 Remobilization of andesite magma by intrusion of mafic magma at the Soufriere Hills Volcano,
650 Montserrat, West Indies, *J. Petrol.*, 41, 21-42, doi:10.1093/petrology/41.1.21, 2000.

- 651 Murray, B. J., Broadley, S. L., Wilson, T. W., Atkinson, J. D., and Wills, R. H.:
652 Heterogeneous freezing of water droplets containing kaolinite particles, *Atmos. Chem. Phys.*, 11,
653 4191-4207, doi:10.5194/acp-11-4191-2011, 2011.
- 654 Murray, B. J., O'Sullivan, D., Atkinson, J. D., and Webb, M. E.: Ice nucleation by particles
655 immersed in supercooled cloud droplets, *Chem. Soc. Rev.*, 41, 6519-6554,
656 doi:10.1039/c2cs35200a, 2012.
- 657 Niemand, M., Moehler, O., Vogel, B., Vogel, H., Hoose, C., Connolly, P., Klein, H.,
658 Bingemer, H., DeMott, P., Skrotzki, J., and Leisner, T.: A Particle-Surface-Area-Based
659 Parameterization of Immersion Freezing on Desert Dust Particles, *J. Atmos. Sci.*, 69, 3077-3092,
660 doi:10.1175/jas-d-11-0249.1, 2012.
- 661 Pinti, V., Marcolli, C., Zobrist, B., Hoyle, C. R., and Peter, T.: Ice nucleation efficiency of
662 clay minerals in the immersion mode, *Atmos. Chem. Phys.*, 12, 5859-5878, doi:10.5194/acp-12-
663 5859-2012, 2012.
- 664 Robock, A.: Climatic Impact of Volcanic Emissions, in: *The State of the Planet: Frontiers*
665 *and Challenges in Geophysics*, American Geophysical Union, Washington, D.C., 125-134, 2004.
- 666 Rose, W. I., Anderson, A. T., Woodruff, L. G., and Bonis, S. B.: October 1974 basaltic
667 tephra from fuego volcano—description and history of magma body, *J. Volcanol. Geoth. Res.*, 4,
668 3-53, doi:10.1016/0377-0273(78)90027-6, 1978.
- 669 Rose, W. I., Bluth, G. J. S., Schneider, D. J., Ernst, G. G. J., Riley, C. M., Henderson, L.
670 J., and McGimsey, R. G.: Observations of volcanic clouds in their first few days of atmospheric
671 residence: The 1992 eruptions of Crater Peak, Mount Spurr volcano, Alaska, *J. Geol.*, 109, 677-
672 694, doi:10.1086/323189, 2001.
- 673 Rose, W. I., and Durant, A. J.: Fate of volcanic ash: Aggregation and fallout, *Geology*, 39,
674 895-896, doi:10.1130/focus092011.1, 2011.
- 675 Schill, G. P., and Tolbert, M. A.: Heterogeneous ice nucleation on phase-separated organic-
676 sulfate particles: effect of liquid vs. glassy coatings, *Atmos. Chem. Phys.*, 13, 4681-4695,
677 doi:10.5194/acp-13-4681-2013, 2013.
- 678 Schnell, R. C., and Delany, A. C.: Airborne ice nuclei near an active volcano, *Nature*, 264,
679 535-536, doi:10.1038/264535a0, 1976.
- 680 Schultz, D. M., Kanak, K. M., Straka, J. M., Trapp, R. J., Gordon, B. A., Zrnica, D. S.,
681 Bryan, G. H., Durant, A. J., Garrett, T. J., Klein, P. M., and Lilly, D. K.: The mysteries of
682 mammatus clouds: Observations and formation mechanisms, *J. Atmos. Sci.*, 63, 2409-2435,
683 doi:10.1175/jas3758.1, 2006.

684 [Seifert, P., Ansmann, A., Gross, S., Freudenthaler, V., Heinold, B., Hiebsch, A., Mattis, I.,](#)
685 [Schmidt, J., Schnell, F., Tesche, M., Wandinger, U., and Wiegner, M.: Ice formation in ash-](#)
686 [influenced clouds after the eruption of the Eyjafjallajokull volcano in April 2010, *J. Geophys.*](#)
687 [Res.-Atmos., 116, doi:10.1029/2011jd015702, 2011.](#)

688 Sihvonen, S. K., Schill, G. P., Lykтей, N. A., Veghte, D. P., Tolbert, M. A., and Freedman,
689 M. A.: Chemical and Physical Transformations of Aluminosilicate Clay Minerals Due to Acid
690 Treatment and Consequences for Heterogeneous Ice Nucleation, *J. Phys. Chem. A*, 118, 8787-
691 8796, doi:10.1021/jp504846g, 2014.

692 Small, C., and Naumann, T.: The global distribution of human population and recent
693 volcanism, *Environ. Hazards*, 3, 93-109, doi:10.3763/ehaz.2001.0309, 2001.

694 Steinke, I., Moehler, O., Kiselev, A., Niemand, M., Saathoff, H., Schnaiter, M., Skrotzki,
695 J., Hoose, C., and Leisner, T.: Ice nucleation properties of fine ash particles from the
696 Eyjafjallajokull eruption in April 2010, *Atmos. Chem. Phys.*, 11, 12945-12958, doi:10.5194/acp-
697 11-12945-2011, 2011.

698 Sullivan, R. C., Moore, M. J. K., Petters, M. D., Kreidenweis, S. M., Qafoku, O., Laskin,
699 A., Roberts, G. C., and Prather, K. A.: Impact of Particle Generation Method on the Apparent
700 Hygroscopicity of Insoluble Mineral Particles, *Aerosol Sci. Tech.*, 44, 830-846,
701 doi:10.1080/02786826.2010.497514, 2010.

702 Todoli, J. L., and Mermet, J. M.: *Liquid Sample Introduction in ICP Spectrometry: A*
703 *Practical Guide*, Elsevier Science, the Netherlands, 2011.

704 Vali, G., and Stansbury, E. J.: Time-dependent characteristics of heterogeneous nucleation
705 of ice, *Can. J. Phys.*, 44, 477-502, 1966.

706 Vali, G.: Freezing rate due to heterogeneous nucleation, *J. Atmos. Sci.*, 51, 1843-1856,
707 doi:10.1175/1520-0469(1994)051<1843:frdthn>2.0.co;2, 1994.

708 Vali, G.: Repeatability and randomness in heterogeneous freezing nucleation, *Atmos.*
709 *Chem. Phys.*, 8, 5017-5031, doi:10.5194/acp-8-5017-2008, 2008.

710 Van Eaton, A. R., Muirhead, J. D., Wilson, C. J. N., and Cimarelli, C.: Growth of volcanic
711 ash aggregates in the presence of liquid water and ice: an experimental approach, *B. Volcanol.*,
712 74, 1963-1984, doi:10.1007/s00445-012-0634-9, 2012.

713 Wilson, C. J. N., Blake, S., Charlier, B. L. A., and Sutton, A. N.: The 26.5 ka Oruanui
714 eruption, Taupo volcano, New Zealand: Development, characteristics and evacuation of a large
715 rhyolitic magma body, *J. Petrol.*, 47, 35-69, 2006.

716 Wise, M. E., Baustian, K. J., and Tolbert, M. A.: Internally mixed sulfate and organic
717 particles as potential ice nuclei in the tropical tropopause region, *P. Natl. Acad. Sci. USA*, 107,
718 6693-6698, doi:10.1073/pnas.0913018107, 2010.

719 Witham, C. S., Oppenheimer, C., and Horwell, C. J.: Volcanic ash-leachates: a review and
720 recommendations for sampling methods, *J. Volcanol. Geoth. Res.*, 141, 299-326,
721 doi:10.1016/j.jvolgeores.2004.11.010, 2005.

722 Yakobi-Hancock, J. D., Ladino, L. A., and Abbatt, J. P. D.: Feldspar minerals as efficient
723 deposition ice nuclei, *Atmos. Chem. Phys.*, 13, 11175-11185, doi:10.5194/acp-13-11175-2013,
724 2013.

725 Zolles, T., Burkart, J., Häusler, T., Pummer, B., Hitzenberger, R., and Grothe, H.:
726 Identification of Ice Nucleation Active Sites on Feldspar Dust Particles, *J. Phys. Chem. A*, 119,
727 2692-2700, doi:10.1021/jp509839x, 2015.